

Effective diffusion tensor computed by homogenization

Dang Van Nguyen¹, Denis Grebenkov², Cyril Poupon³, Denis Le Bihan³, and Jing-Rebecca Li⁴

¹*CMAP, Ecole Polytechnique, Palaiseau, France*, ²*LPMC, CNRS – Ecole Polytechnique, Palaiseau, France*, ³*Neurospin, CEA Saclay, Gif-sur-Yvette, France*, ⁴*Equipe DEFI, INRIA Saclay, Palaiseau, France*

Corresponding author: Dang Van Nguyen, E-Mail: vdnguyen@cmap.polytechnique.fr

Abstract

The convergence of the long-time apparent diffusion tensor of diffusion magnetic resonance imaging (dMRI) to the effective diffusion tensor obtained by mathematical homogenization theory was considered for two-compartment geometric models containing non-elongated cells of general shapes. A numerical study was conducted in two and three dimensions to demonstrate this convergence as a function of the diffusion time.

Keywords

Effective diffusion tensor, apparent diffusion tensor, two-compartment model, Bloch-Torrey equation, Laplace equation.

1. Introduction

Diffusion magnetic resonance imaging (dMRI) can give useful information on cellular structure and structural changes [1]. We show that the effective diffusion tensor obtained by mathematical homogenization theory [2,3] gives a good approximation to the long-time apparent diffusion tensor of dMRI for two-compartment geometrical models containing non-elongated cells of general shapes. The homogenized diffusion tensor is obtained by solving d steady-state Laplace equations (where $d = 2,3$ is the problem dimension), which is a more computationally efficient approach than time-consuming simulations in the time domain, either via Monte-Carlo simulation or numerical solution of the time-dependent Bloch-Torrey PDE.

2. Theory

We consider two compartments, Ω^{in} and Ω^{ex} , to be an ensemble of cells and the extra-cellular space, respectively, with the same intrinsic diffusion coefficient D . The cell membranes are modeled by an infinitely thin permeable interface Γ characterized by a permeability κ . Fig. 1 illustrates a 2D example in which the union of blue cells is considered as the interior compartment and the remaining part is the exterior.

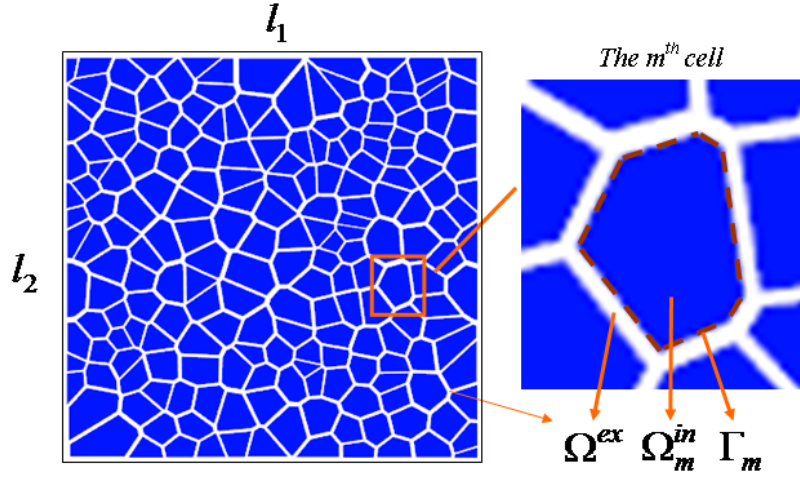


Fig. 1: A two-compartment model with the extracellular compartment Ω^{ex} (white region), the intracellular compartment $\Omega^{in} = \cup_m \Omega_m^{in}$ (blue regions) and the interface $\Gamma = \cup_m \Gamma_m$

For a given diffusion-encoding magnetic field gradient with the temporal profile $f(t)$, gradient vector \vec{g} and the gyromagnetic ratio γ , the transverse magnetization is described by the two-compartment Bloch-Torrey partial differential equation (PDE) [4]

$$\frac{\partial M(\vec{x}, t)}{\partial t} = -i \gamma f(t) (\vec{g} \cdot \vec{x}) M(\vec{x}, t) + \nabla (D \nabla M(\vec{x}, t)) \quad (1)$$

for $M=M^{in}$ and $M=M^{ex}$ and with boundary conditions at the inter-compartment interface Γ :

$$D \nabla M^{in}(\vec{x}, t) \cdot \vec{n}^{in}(\vec{x}) = -D \nabla M^{ex}(\vec{x}, t) \cdot \vec{n}^{ex}(\vec{x}) = \kappa (M^{ex}(\vec{x}, t) - M^{in}(\vec{x}, t)), \quad \vec{x} \in \Gamma, \quad (2)$$

(here \vec{n}^{ex} and \vec{n}^{in} are normal vectors at Γ pointing outward Ω^{ex} and Ω^{in} , respectively), and

the boundary conditions at the exterior boundaries of the computational box $\Omega = \prod_{k=1}^d [a_k, b_k]$,

($a_k < b_k$) which contains a representative sample of the cellular structure:

$$\begin{aligned} [M(\vec{x}, t)]_{x_k=a_k} &= [M(\vec{x}, t)]_{x_k=b_k} \exp\left(i (\vec{g} \cdot \vec{e}_k) \gamma l_k \int_0^t f(s) ds\right) \\ \left[\frac{\partial M(\vec{x}, t)}{\partial x_k}\right]_{x_k=a_k} &= \left[\frac{\partial M(\vec{x}, t)}{\partial x_k}\right]_{x_k=b_k} \exp\left(i \gamma (\vec{g} \cdot \vec{e}_k) l_k \int_0^t f(s) ds\right) \end{aligned} \quad (3)$$

where $l_k = b_k - a_k$, $k = 1..d$, $\vec{x} = (x_1, \dots, x_d)$ is the spatial position, and \vec{e}_k is the unit vector in the k^{th} coordinate direction.

For the uniform initial condition, the dMRI signal attenuation is computed by

$$\Psi(\vec{g}, t) = \int_{\Omega} M(\vec{x}, t) d\vec{x} \quad (4)$$

and is usually plotted against the b-value:

$$b = \gamma^2 \|\vec{g}\|^2 \int_0^t \left(\int_0^u f(s) ds \right)^2 du \quad (5)$$

We also denote \vec{q} the gradient direction: $\vec{q} = \vec{g} / \|\vec{g}\|$.

From the Taylor expansion of the dMRI signal in b-value, we define the apparent diffusion tensor D^A which may depend on time t:

$$\ln \Psi(\vec{g}, t) = -bD^A + O(\|\vec{g}\|^2) \quad (6)$$

The long-time limit of D^A can be approximated by the effective diffusion tensor obtained from homogenization theory [6], $D^{eff} = [D_{jk}^{eff}]_{j=1..d, k=1..d}$,

$$D_{jk}^{eff} = D \int_{\Omega} \nabla v_j \cdot \vec{e}_k \, d\vec{x} \quad (7)$$

where the functions v_j can be found by solving the Laplace equation

$$-\nabla(D\nabla v_j(\vec{x})) = 0 \quad (8)$$

with the boundary conditions at the inter-compartment interface Γ ,

$$D\nabla v_j^{in}(\vec{x}) \cdot \vec{n}^{in}(\vec{x}) = -D\nabla v_j^{ex}(\vec{x}) \cdot \vec{n}^{ex}(\vec{x}) = \kappa \left(v_j^{ex}(\vec{x}) - v_j^{in}(\vec{x}) \right), \quad \vec{x} \in \Gamma \quad (9)$$

and the boundary conditions at the exterior boundaries of the computational box Ω are

$$\begin{aligned} [v_j(\vec{x})]_{x_k=a_k} &= [v_j(\vec{x})]_{x_k=b_k} - (\vec{g} \cdot \vec{e}_k) l_k \\ \left[\frac{\partial v_j(\vec{x})}{\partial x_k} \right]_{x_k=a_k} &= \left[\frac{\partial v_j(\vec{x})}{\partial x_k} \right]_{x_k=b_k} \end{aligned} \quad (10)$$

In fact, the Laplace equation (8) with the conditions (9) and (10) is just a long-time limit of the Bloch-Torrey equation (1) with the boundary conditions (2) and (3). So, their boundary conditions are similar.

3. Materials and Methods

We solved the Bloch-Torrey equation and the Laplace equation using a linear finite element method relying on the Fenics (www.fenicsproject.org) platform for PDE formulation using finite elements and the Salomé (www.salome-platform.org) platform for mesh generation. We considered here a computational domain $[-10\mu m, 10\mu m]^d$ containing numerous non-elongated cells. To construct these samples, we randomly generated a set of segments in 2D and a set of faces in 3D. Since the boundaries should be periodic, we mirrored this set across all coordinate axes. Then, each segment (face) was thickened to create an extracellular compartment Ω^{ex} . The interior compartment Ω^{in} includes the remaining polygonal (2D) or polyhedral (3D) cells.

The 2D sample was created by 20 thick segments that divided the computational domain into 116 convex cells (Fig. 2) with the volume fraction $v^i = 0,77$, the average radius of cells $1,2\mu m$ and the average surface to volume ratio $S/V = 0,41\mu m^{-1}$. Similarly, the 3D sample was created by 16 thick faces which cut the cube into 80 cells (Fig. 3) with the average radius of cells $2,5\mu m$, volume fraction $v^i = 0,66$ and the average surface to volume ratio $S/V = 0,29\mu m^{-1}$.

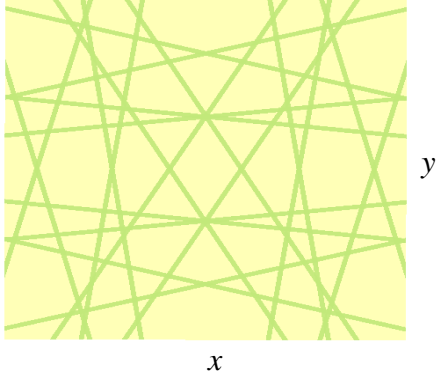


Fig.2: 2D sample

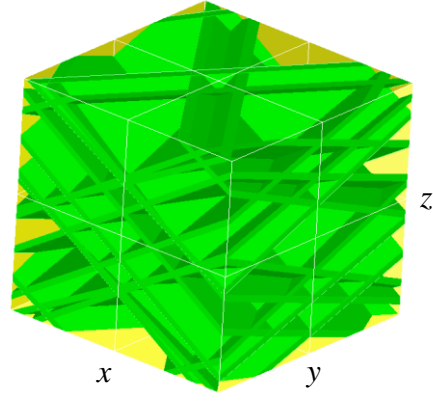


Fig.3: 3D sample

The same intrinsic diffusion coefficient of water molecules $D = 3 \cdot 10^{-3} \frac{\mu\text{m}^2}{\mu\text{s}}$ was set for both interior and exterior compartments. Two values of permeability, $\kappa = 10^{-5} \frac{\mu\text{m}}{\mu\text{s}}$ and $\kappa = 10^{-4} \frac{\mu\text{m}}{\mu\text{s}}$, were considered.

The Bloch-Torrey equation (1) with the conditions (2) and (3) was solved for Stejskal - Tanner PGSE sequences (Fig. 4) with two rectangular gradient pulses of duration $\delta = 10\text{ms}$ and several diffusion times Δ to obtain the signal attenuation $\Psi(\vec{g}, t)$ at some b-values, $b = \gamma^2 \|\vec{g}\|^2 \delta^2 \left(\Delta - \frac{\delta}{3} \right)$.

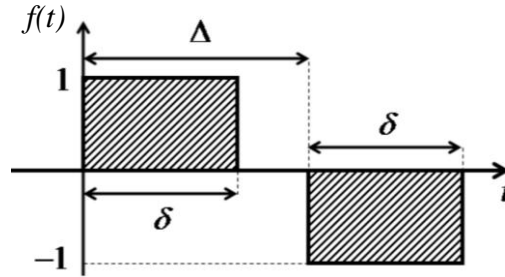


Fig.4: Stejskal-Tanner PGSE

Then, the entries of D^A appear in front of the first-order term of the polynomial fit of $-\ln \Psi(\vec{g}, t)$ versus b-value.

The Laplace equation (8) with conditions (9) and (10) was also solved over the same sample to obtain D^{eff} by (7).

All computations were carried out on a Dell Latitude E6410 laptop computer.

4. Results

The 2D and 3D simulations on two samples shown on Fig.2 and Fig.3 are presented in this section.

2D simulations

We performed the simulations for two gradient directions $[1,0]$ and $[0,1]$. Each D^A was computed from 7 b-values changing from 0 to $4000 \frac{\mu\text{s}}{\mu\text{m}^2}$ for $\kappa = 10^{-5} \frac{\mu\text{m}}{\mu\text{s}}$, and from 0 to

$3000 \frac{\mu\text{s}}{\mu\text{m}^2}$ for $\kappa = 10^{-4} \frac{\mu\text{m}}{\mu\text{s}}$ that took between 15 and 30 minutes for the mesh size of 33813 vertices. On the contrary, it took only a few seconds to compute each D^{eff} on the same mesh.

Figure 5 shows the convergence of D^A to D^{eff} for the first direction [1,0] and the permeability $\kappa = 10^{-5} \frac{\mu\text{m}}{\mu\text{s}}$ with 10 values of diffusion time Δ changing from 10ms to 190ms. We plot here the diffusion coefficient versus Δ^{-1} .

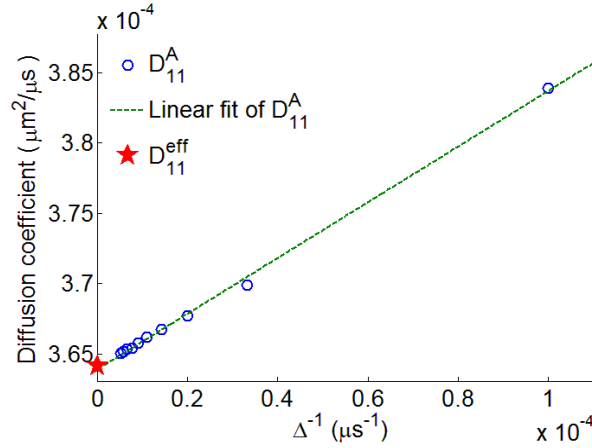


Fig.5: The convergence of D^A to D^{eff} in 2D in the direction [1,0] and $\kappa = 10^{-5} \frac{\mu\text{m}}{\mu\text{s}}$. The blue circles represents D^A , the dashed line shows a linear fit of D^A versus Δ^{-1} , and the red star indicates D^{eff} .

More results in two gradient directions [1,0] and [0,1], three diffusion times $\Delta=10\text{ms}$, 50ms and 190ms and two permeabilities $\kappa=10^{-4} \mu\text{m}/\mu\text{s}$, and $10^{-5} \mu\text{m}/\mu\text{s}$ are in Table 1.

Table 1. Summary of results for 2D simulations

	$\kappa=10^{-4} \mu\text{m}/\mu\text{s}$				$\kappa=10^{-5} \mu\text{m}/\mu\text{s}$			
	$\vec{q}^T D^A \vec{q}$			$\vec{q}^T D^{eff} \vec{q}$	$\vec{q}^T D^A \vec{q}$			$\vec{q}^T D^{eff} \vec{q}$
\vec{q}	$\Delta=10$	$\Delta=110$	$\Delta=190$		$\Delta=10$	$\Delta=110$	$\Delta=190$	
[1,0]	$5,33 \cdot 10^{-4}$	$5,24 \cdot 10^{-4}$	$5,23 \cdot 10^{-4}$	$5,22 \cdot 10^{-4}$	$3,84 \cdot 10^{-4}$	$3,66 \cdot 10^{-4}$	$3,65 \cdot 10^{-4}$	$3,64 \cdot 10^{-4}$
[0,1]	$5,69 \cdot 10^{-4}$	$5,61 \cdot 10^{-4}$	$5,60 \cdot 10^{-4}$	$5,59 \cdot 10^{-4}$	$4,06 \cdot 10^{-4}$	$3,95 \cdot 10^{-4}$	$3,94 \cdot 10^{-4}$	$3,93 \cdot 10^{-4}$

3D simulations

The simulations were performed for three gradient directions [1,0,0], [0,1,0] and [0,0,1]. Each D^A was computed at 9 b-values changing from 0 to $3000 \frac{\mu\text{s}}{\mu\text{m}^2}$ for $\kappa = 10^{-5} \frac{\mu\text{m}}{\mu\text{s}}$, and from 0 to $2000 \frac{\mu\text{s}}{\mu\text{m}^2}$ for $\kappa = 10^{-4} \frac{\mu\text{m}}{\mu\text{s}}$. The computation took between 30 minutes and 2 hours for each D^A on the mesh size of 50476 vertices. On the contrary, it took less than one minute to compute D^{eff} on the same mesh.

Five values of the diffusion time Δ , 10ms, 30ms, 50ms and 90ms, were chosen to study the convergence of D^A to D^{eff} for the first direction [1,0,0] and $\kappa = 10^{-5} \frac{\mu\text{m}}{\mu\text{s}}$. The corresponding D^A was shown versus Δ^{-1} in Fig. 6.

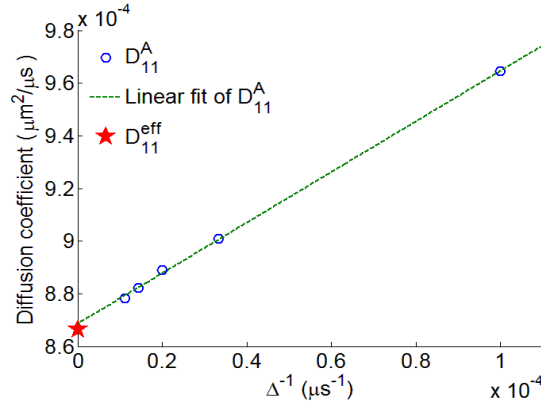


Fig. 6: The convergence of D^A to D^{eff} in 3D for the direction $[1,0,0]$ and $\kappa = 10^{-5} \frac{\mu m}{\mu s}$. The blue circles represents D^A , the dashed line shows a linear fit of D^A versus Δ^{-1} , and the red star indicates D^{eff} .

More results for three gradient directions $[1,0,0]$, $[0,1,0]$ and $[0,0,1]$, three diffusion times $\Delta=10\text{ms}$, 50ms and 90ms and two permeabilities $\kappa=10^{-4} \mu m/\mu s$ and $\kappa=10^{-5} \mu m/\mu s$ are summarized in Table 2.

Table 2. Summary of results for 3D simulations

\vec{q}	$\kappa=10^{-4} \mu m/\mu s$				$\kappa=10^{-5} \mu m/\mu s$			
	$\vec{q}^T D^A \vec{q}$			$\vec{q}^T D^{eff} \vec{q}$	$\vec{q}^T D^A \vec{q}$			$\vec{q}^T D^{eff} \vec{q}$
	$\Delta=10$	$\Delta=50$	$\Delta=90$		$\Delta=10$	$\Delta=50$	$\Delta=90$	
$[1,0,0]$	$1,24 \cdot 10^{-3}$	$1,22 \cdot 10^{-3}$	$1,22 \cdot 10^{-3}$	$1,21 \cdot 10^{-3}$	$9,65 \cdot 10^{-4}$	$8,89 \cdot 10^{-4}$	$8,78 \cdot 10^{-4}$	$8,66 \cdot 10^{-4}$
$[0,1,0]$	$1,73 \cdot 10^{-3}$	$1,67 \cdot 10^{-3}$	$1,67 \cdot 10^{-3}$	$1,66 \cdot 10^{-3}$	$1,26 \cdot 10^{-3}$	$1,11 \cdot 10^{-3}$	$1,09 \cdot 10^{-3}$	$1,07 \cdot 10^{-3}$
$[0,0,1]$	$6,89 \cdot 10^{-4}$	$6,87 \cdot 10^{-4}$	$6,85 \cdot 10^{-4}$	$6,85 \cdot 10^{-4}$	$5,01 \cdot 10^{-4}$	$4,93 \cdot 10^{-4}$	$4,92 \cdot 10^{-4}$	$4,91 \cdot 10^{-4}$

5. Discussion and conclusion

The results in Figures 5, 6 and Tables 1, 2 show that the long-time apparent diffusion tensor D^A approaches the steady-state tensor D^{eff} computed by the homogenization for PGSE sequences in both cases of isotropic and anisotropic diffusion. The convergence is faster at higher permeability and seems to be linear in term of Δ^{-1} that agrees with the result for 1D periodic structure in the long-time regime [7]. This approach can be applied to general geometrical shapes, as long as a good mesh can be generated. Other diffusion-encoding pulse sequences may be used, as long as the diffusion time is long. The computation of D^{eff} is much faster than that of D^A . We expect that the experimentally obtained apparent diffusion tensors can be used to estimate D^{eff} by extrapolation in Δ^{-1} , and then information, obtained analytically or numerically, about D^{eff} can be used to infer the properties of the imaged sample.

References

- [1] LeBihan (2007) Phys Med Bio 52.
- [2] Bensoussan et al. (1978) Asymptotic analysis for periodic structures, North-Holland, Amsterdam.
- [3] Cheng et al. (1997) Proc Math Phy Engin Sci 453:145–161.
- [4] Grebenkov (2007) Rev Mod Phys 79, 1077–1137.
- [5] Novikov et al. (2011) Nature Physics 7, 508–514.
- [6] Li et al. (preprint) Numerical and analytical models of the long time apparent diffusion tensor.
- [7] Yablonskiy et al. (2010) NMR Biomed 23, 661–681.